Understanding the Visible Absorption of Electron Accepting and Donating CNDs

Yana Reva, Bikash Jana,* Daniel Langford, Marina Kinzelmann, Yifan Bo, Peter R. Schol, Tobias Scharl, Xinyi Zhao, Ryan W. Crisp, Thomas Drewello, Timothy Clark, Alejandro Cadranel,* and Dirk M. Guldi*

Carbon nanodots (CNDs) synthesized from citric acid and formyl derivatives, that is, formamide, urea, or *N*-methylformamide, stand out through their broad-range visible-light absorbance and extraordinary photostability. Despite their potential, their use has thus far been limited to imaging research. This work has now investigated the link between CNDs' photochemical properties and their chemical structure. Electron-rich, yellow carbon nanodots (yCNDs) are obtained with in situ addition of NaOH during the synthesis, whereas otherwise electron-poor, red carbon nanodots (rCNDs) are obtained. These properties originate from the reduced and oxidized dimer of citrazinic acid within the matrix of yCNDs and rCNDs, respectively. Remarkably, yCNDs deposited on TiO$_2$ give a 30% higher photocurrent density of 0.7 mA cm^{-2} at +0.3 V versus Ag/AgCl under Xe-lamp irradiation (450 nm long-pass filter, 100 mW cm^{-2}) than rCNDs. The difference in overall photoelectric performance is due to fundamentally different charge-transfer mechanisms. These depend on either the electron-accepting or the electron-donating nature of the CNDs, as is evident from photoelectrochemical tests with TiO$_2$ and NiO and time-resolved spectroscopic measurements.

1. Introduction

To overcome the challenge of utilizing solar light irradiation, state-of-the-art nanomaterials that are not only efficient, but also environmentally friendly and cost-saving are being sought.[1] In recent years, carbon nanodots (CNDs) have been considered to be a potential material for visible-light utilization.[2] CNDs, which consist solely of earth-abundant elements such as C, N, and O, are readily produced from inexpensive and environmental friendly precursors, such as citric[3] or tartaric acid[4] using various methods, such as microwave irradiation,[5] vacuum-heating,[6] or solvothermal[7] reactions. Among these methods, solvothermal synthesis is easily accessible under laboratory conditions since only simple equipment is required.[8] Non-π-conjugated precursors

Y. Reva, B. Jana, D. Langford, Y. Bo, P. R. Schol, T. Scharl, X. Zhao,
A. Cadranel, D. M. Guldi
Department of Chemistry and Pharmacy & Interdisciplinary
Center for Molecular Materials (ICMM)
Physical Chemistry I
Friedrich-Alexander-Universität Erlangen-Nürnberg
Egerlandstraße 3, 91058 Erlangen, Germany
E-mail: bikash.jana@campus.technion.ac.il;
ale.cadranel@fau.de; dirk.guldi@fau.de
B. Jana
Technion – Israel Institute of Technology
Schulich Faculty of Chemistry
Technion
Haifa 3200008, Israel

M. Kinzelmann, T. Drewello
Department of Chemistry and Pharmacy
Physical Chemistry I
Friedrich-Alexander-Universität Erlangen-Nürnberg
Egerlandstraße 3, 91058 Erlangen, Germany
Y. Bo, T. Clark
Department of Chemistry and Pharmacy
Computer-Chemistry Center
Friedrich-Alexander-Universität Erlangen-Nürnberg
Nägelsbachstrasse 25, 91052 Erlangen, Germany
X. Zhao
College of Chemistry and Chemical Engineering
Central South University
Changsha, Hunan 410083, China
R. W. Crisp
Department of Chemistry and Pharmacy
Chair of Chemistry of Thin Film Materials
Friedrich-Alexander-Universität Erlangen-Nürnberg
Cauerstraße 3, 91058 Erlangen, Germany

ADVANCED
SCIENCE NEWS
www.advancedsciencenews.com

NANO · MICRO
small
www.small-journal.com

in the solvothermal reaction result mainly in UV-light absorbing CNDs with low extinction coefficient features in the visible region. A notable exception are visible-light absorbing CNDs, whose main absorption extends up to 550 nm.[9] These are synthesized from citric acid and urea in formamide or *N*-methylformamide.[10]

Previous studies addressing the structure of visible light absorbing CNDs attributed the unique photophysical properties to the limited dimensionality of the π-conjugated sp²-domains[11] and a certain grade of nitrogen doping.[12] Quantum confinement properties and a graphitic core structure are implicit. This assumption is, however, largely controversial. Recent reports suggest, for example, that molecular chromophores in CNDs contribute to the red-absorbing properties. For instance, Liang et al.[13] obtained the red coloration by processing citric acid with formamide at 135 °C. 135 °C is, however, far below the carbonization temperature of at least 300 °C.[14] Visible-light absorption was also obtained by processing citric acid with N-H amide-functionalized reactants. Peralkylation of the N-centers of amides, as in the case of in *N,N,N′N′*-tetramethylurea and *N,N*-dimethylformamide (DMF), failed to give any red-absorbing spectral features.[13] Therefore, it is reasonable to assume that the visible light absorptions originate from chemical reactions involving the N-centers of amides to form N-hetero-π-conjugated molecular chromophores. Furthermore, to date, the fundamental composition of visible light-absorbing CNDs is still unknown and their applications are restricted to bioimaging.[9,15]

Here, we address the structure of CNDs synthesized from citric acid and formamide, with in situ or post-synthetic treatment with NaOH using various experimental techniques. Insights from mass spectrometry (MS) and redox-characterization reveal that the coloration in red carbon nanodots (rCNDs) stems from an oxidized form of dimerized citrazinic acid, while the spectral features of yellow carbon nanodots (yCNDs) can be traced back to a reduced form of the citrazinic acid dimer, obtained after in situ treatment with NaOH. In addition, several structural and optical investigations reveal the presence of molecular chromophores in CNDs. Finally, CND-based photoanodes allowed us to obtain excellent and stable photocurrents and proceed with the photoelectrochemical analyses. Incident-photon-to-current efficiency (IPCE) and electrochemical impedance spectroscopy (EIS) revealed different injection-behaviors for the two different CNDs. The intrinsic electron–donor and –acceptor characteristics were therefore evaluated with TiO₂ and NiO, respectively, by means of chrono-amperometric measurements. Our work was rounded off by time-resolved optical spectroscopy, which led to deeper insights into the processes occurring at photoanodes decorated with CNDs.

2. Results and Discussion

2.1. Synthesis and Basic Characterization

rCNDs were prepared from a formamide solution of citric acid and ethylenediamine using a solvothermal procedure in a Teflon-lined stainless-steel autoclave. The reaction conditions were 180 °C for 6 h (details are given in the Supporting Information).[9] The crude product was centrifuged and treated with acetone and an aqueous NaOH solution (2 M) to remove undesired residuals, giving rCNDs. We altered the synthesis procedure to obtain the in situ modified yCNDs, by adding NaOH to the precursor mixture prior to any autoclave heating. The product was purified via dialysis (500 Da in deionized water) for 24 h and dried with a rotary evaporator at 45 °C.

In water, rCNDs show absorption maxima at 345 and 520 nm. Addition of NaOH to the precursor solution afforded yCNDs with different spectral properties. A 350 nm maximum and a 420 nm shoulder are discernable. These features become more distinct as the in situ added NaOH concentration is increased. At the same time, the 520 nm absorption becomes 90% less intense and red-shifts to 550 nm (**Figure 1**a). Notably, addition of more than 250 mg NaOH to the reaction mixture prior to autoclaving resulted in minor changes in the absorption spectra. We therefore opted for 250 mg of NaOH in the preparation of yCNDs.

Excitation-emission maps were recorded to gain additional insight into the photoexcited features of rCND and yCND (Figure 1b,c). Photoexcitation at 400 nm resulted in two emissive features: 450 and 650 nm maxima for rCND (Figure 1b), and 450 and 550 nm maxima for yCND (Figure 1c). Photoexciting rCND and yCND at 550 nm, on the other hand, resulted in only one emission maximum at 625 nm. Recent
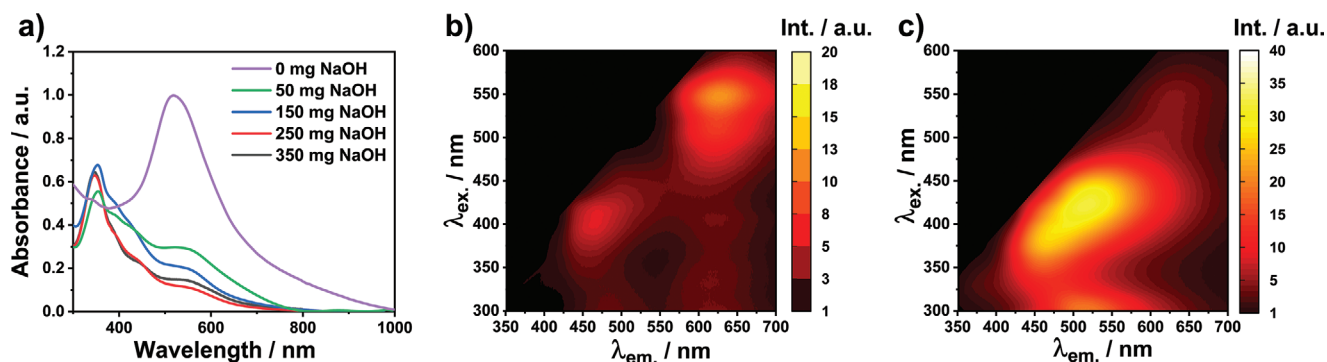

Figure 1. a) Absorption spectra of CNDs in water ($c = 0.05$ mg mL⁻¹) synthesized with different amount of NaOH added in situ. Excitation-emission mapping of b) rCNDs ($c = 0.02$ mg mL⁻¹) and c) yCNDs ($c = 0.05$ mg mL⁻¹) in water.

reports suggest that the absorption and emission in the visible range originate from molecular chromophores formed by citric acid and formamide.[13]

The Raman spectra revealed information regarding the degree of CND graphitization (Figure S1, Supporting Information). The intensities of the D- and G-bands were used to estimate the graphitic defect density.[16] Raman scattering showed multiple bands for rCND and yCNDs, whose analysis required multiband fitting.[17] In accordance with the five-band fit proposed by Sadezky et al.,[18] the G-, D*-, D**-, D-, and D′-bands at 1548, 1297, 1463, 1347, and 1624 cm^{-1}, respectively, were fitted with Lorentzian functions. The D-to-G intensity ratio is 1.27 for yCND, and 1.45 for rCND, suggesting that rCNDs are more amorphous than yCNDs.

Both CNDs are paramagnetic and electron paramagnetic resonance (EPR) active with g-factor of 2.001. rCNDs with a 12 times higher signal are more EPR active (Figure S2, Supporting Information). We plotted the normalized EPR intensity versus the square root of the microwave power to gain insight into the structural environment of the organic radicals. In yCND, the microwave power saturated at 0.1 W$^{1/2}$, which suggests less structural disorder in the organic material, compared to rCND, where the maximum is reached at 0.2 W$^{1/2}$ (Figure S2, Supporting Information).

The X-ray diffraction (XRD) patterns for rCNDs and yCNDs are nearly identical in terms of their broad reflections centered at ≈23° (Figure S3, Supporting Information). Similarly, solvothermally synthesized CNDs are characterized as well by broad reflections between 20° and 30°.[19]

To gain further insights into the nanoparticle formation and to characterize their sizes, atomic force microscopy (AFM) was conducted. Corresponding profiles reveal an average height of 1.4 nm for rCNDs and almost half of it for yCNDs, that is, 0.7 nm (Figure S4, Supporting Information).

2.2. Molecular Insights

Recent studies on the formation of CNDs from either ethylenediamine or urea in combination with citric acid have suggested that a ring-closing reaction between amines and carboxylic acids during the solvothermal preparation of CNDs produces citrazinic acid (**1**) and other molecular fluorophores.[20–23] Therefore, it is reasonable to expect a similar reaction between citric acid and formamide. The mass spectrum of rCND (**Figure 2**) reveals peaks at m/z 155, 154, and 139. The first two correspond to **1** (M = 155 g mol^{-1}) and its radical **1•** (M = 154 g mol^{-1}), while the latter relates to the *N*-formylated decarboxylated form of **1** (**2** in **Figure 3**a). **1•** and **2** are potentially formed from the intermediate shown in Figure 3a. Figure 3c gives an overview of the proposed molecular chromophores. In addition, **3** is formed in a reaction between one equivalent of citric acid and two equivalents of ethylenediamine via ring-closing and amidation reactions. **3** (M = 222 g mol^{-1}) is assigned in the MS experiments to m/z 222 – Figure 2. We assume that ions are formed here during electrospray ionization mass spectrometry (ESI-MS) by electrochemical oxidation rather than protonation, which is common for aliphatic nitrogen compounds.

1 absorbs light, however, at 335 nm in water. The rCND absorption across the visible range is likely to originate from larger π-extended systems produced, for example, upon dimerization of **1** under aerobic conditions. To evaluate the relation of **1** to the visible-light absorption of rCNDs, we performed additional solvothermal synthesis experiments. In particular, we employed the same procedure used for the rCND synthesis, but with **1** as the primary starting material and with DMF as solvent. DMF prevents undesirable amidations, which are generated in the presence of formamide under solvothermal conditions, and hence places the focus on the dimerization. The corresponding product is purified by means of the aforementioned
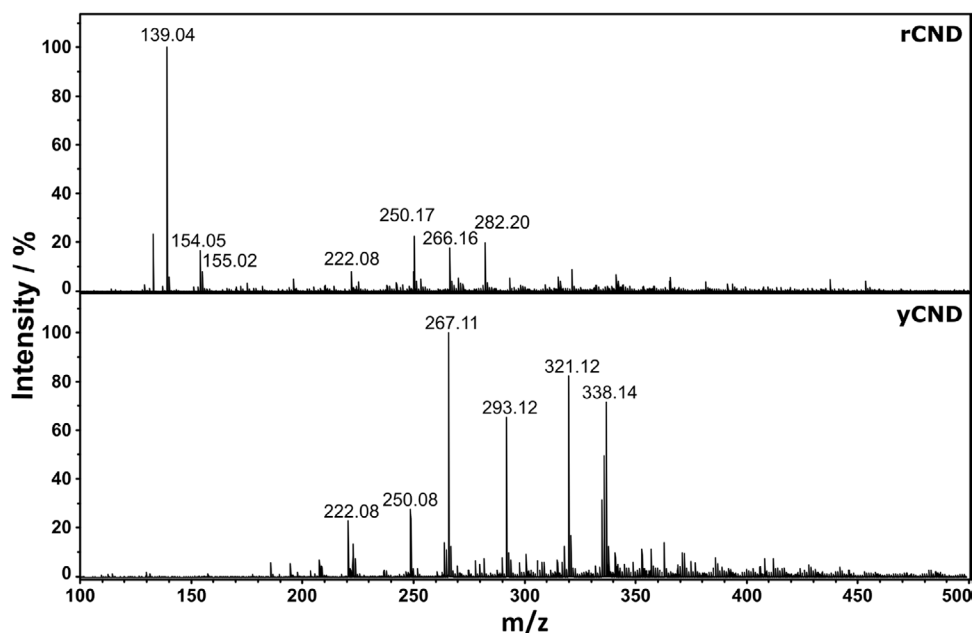

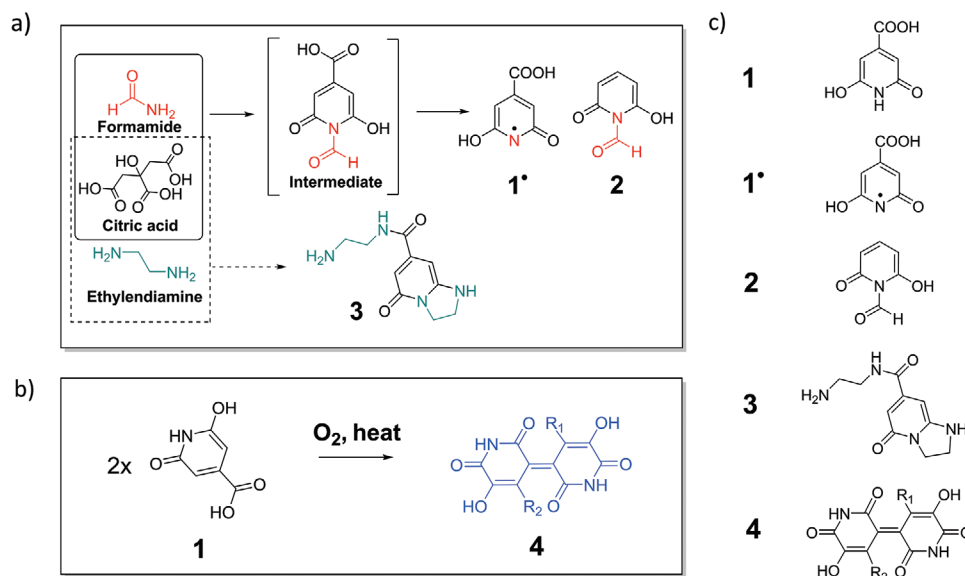**Figure 2.** ESI-MS of CNDs in positive-ion mode.

ADVANCED
SCIENCE NEWS
www.advancedsciencenews.com

NANO · MICRO
small
www.small-journal.com

Figure 3. a) Formation of derivatives of **1** by cyclizing citric acid with N−H containing building blocks. b) Formation of **4** in the presence of oxygen. c) List of the proposed structures.

rCND procedure (see Supporting Information). In water, 508 and 535 nm maxima are in sound agreement with rCNDs (Figure S5, Supporting Information). This finding suggests that the rCND absorption in the visible range stems from a reaction of **1**, presumably a dimerization. In other words, **1** is a key intermediate in the reaction between citric acid and formamide en route to molecular chromophores that are responsible for the absorption of rCNDs in the visible range.

This raised the question of how π-extended systems such as dimers, etc. that absorb in the visible range and that correlate with peaks at m/z 250, 266, and 282 in the MS (Figure 2), are formed from **1**. We therefore repeated the synthesis, but under milder conditions. This included stirring the reaction mixture containing 100 μmol of **1** in 10 mL DMF at room temperature, under ambient pressure, and in the dark. After 1 h, a blue colored product with an absorption at 596 nm in DMF and 568 nm in water evolved (**Figure 4**a,b). Higher temperatures such as 80 °C, accelerate the dimerization of **1** and yield a significantly stronger absorption at 596 nm in DMF (Figure S6, Supporting Information). In line with previous

studies, dimerization of **1** leads to a new class of chromophores, further addressed as **4**, including multiple possible derivatives – Figure 3b.[22a,24] This is in good agreement with the peak at m/z 313 measured for the product synthesized in formamide upon heating to 80 °C for 1 h (Figure S7, Supporting Information). Independent confirmation came from TD-DFT calculations. As an example, we calculated an absorption spectrum for the dimer with substituents R_1=COOH, R_2=OH that is fully consistent with the experimental results (Figure S8, Supporting Information). The MS of rCNDs does not show any signals that can be ascribed to **4**, hence its additional transformations are necessary to yield the molecular chromophores within rCND. With this information at hand, we rationalized the formation of the three high-mass peaks in the MS of rCND at m/z 250, 266, and 282 (Figure 2) and assign them to **5**, **6**, and **7**, respectively (Figure S9, Supporting Information). All of them originate from **4**.

Among all the possible transformations of **4**, we considered its oxidation. In this context, we turned to the chemical oxidation of **4** via a reaction with $Na_2S_2O_8$ in DMF. $Na_2S_2O_8$ was
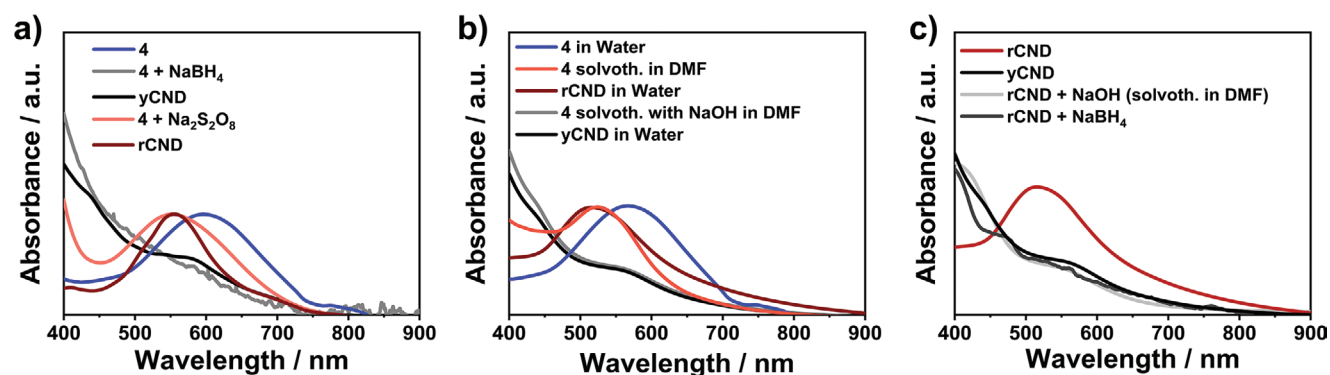

Figure 4. Reductive and oxidative transformations of **4** using a) redox agents in DMF and b) solvothermal processing in DMF (water is generated during solvothermal procedure). c) Transformations of rCNDs into yCNDs by means of redox agent addition and solvothermal treatment in DMF.

ADVANCED
SCIENCE NEWS
www.advancedsciencenews.com

NANO · MICRO
small
www.small-journal.com

selected because it is transparent in the region of interest. Also, $Na_2S_2O_8$ produces $SO_4^{•-}$ radicals, which drive decarboxylations of aromatic carboxylic acids such as those necessary to generate **5**, **6**, and **7** from **4**.[24b] Absorption shifts from 596 to 560 nm (Figure 4a) in DMF go hand-in-hand with the oxidation. The resulting reddish coloration matches that of rCND in DMF (Figure 4a). To ensure that the oxidation under the synthetic conditions affords rCNDs, we treated **4** in DMF solvothermally at 180 °C for 6 h under an inert atmosphere and analyzed the spectral changes. The solvothermally treated **4** turns characteristically red with a 520 nm absorption right after exposure to air. A similar hypsochromic shift develops for the 560 nm absorption in DMF upon addition of traces of water. 520 nm is consistent with the rCND absorption in water, where the maximum evolves at 515 nm (Figure 4b). Although DMF was employed, solvothermal treatment is likely to generate H_2O in situ, causing the solvothermal shift. Next, we turned to spectroelectrochemical oxidation of **4** in DMF. A steadily increasing potential to +0.7 V versus Ag/AgCl evokes a blue-shift of the 580 nm absorption and the development of a 520 nm shoulder. All of this reflects the color change from blue to red as seen for rCNDs (Figure S10, Supporting Information). Hence, we confirmed that oxidative transformations of **4** are linked to the red spectral features seen for rCND.

The same steps were employed to gain insight into the structure of yCNDs. We carried out the synthesis of yCNDs in DMF using **1** as the primary precursor instead of citric acid with the purification procedure described in the Supporting Information. Also for yCNDs, **1** originates molecular chromophores as evident from the absorption spectra with a shoulder at 550 nm, which coincides with the absorbance of yCNDs (Figure S5, Supporting Information).

MS-analysis of yCNDs revealed traces of **1**, **1•**, **2**, and **3** (Figure S9, Supporting Information). Also, several derivatives of **4** are assigned in the yCNDs: **5**, **8•**, **9•**, **9**, **10•**, and **11** (structures are shown in Figure S9, Supporting Information) with their corresponding MS peaks at m/z 250, 267, 293, 294, 321, and 338, respectively – Figure 2. This indicates that the spectral features of yCNDs and rCNDs share the same molecular origin. Signals, found by MS for rCNDs and yCNDs are successfully compared with the calculated isotope pattern (Figures S11 and S12, Supporting Information). To evaluate the involvement of **4** in the formation of yCNDs, we monitored the changes upon reducing **4** with $NaBH_4$ in DMF. Its reduction results in the characteristic yellow coloration. Hereby, the blue-shifted absorption to 573 nm not only coincides with the 574 nm shoulder of yCNDs, but also matches well the entire absorption of yCNDs across the visible range (Figure 4a). **4** was treated solvothermally under similar conditions as used for the synthesis of yCNDs, that is, mixed with 250 mg NaOH and heated to 180 °C for 6 h in DMF in an autoclave. The resulting product shows the same absorption features as yCNDs in water (Figure 4b). Additionally, electrochemical reduction experiments of **4** in DMF (0.5 M $LiClO_4$) are consistent with the results obtained from the chemical reduction using $NaBH_4$ in DMF. After surpassing −1.6 V versus Ag/AgCl, the 580 nm absorption intensifies, blue shifts, and gives the 573 nm shoulder. The latter is fully consistent with the absorbance seen for yCNDs in DMF (Figure S10, Supporting Information).

To sum up, oxidative transformations of **4** lead to the characteristic red coloration distinctive for rCND. Reductive transformations of **4** result in the characteristic yellow coloration of yCNDs. Hence, we conclude that the unique photophysical properties of CNDs originate from the oxidized and reduced dimers of rCNDs and yCNDs, respectively. It is, however, not possible to recover **4** by means of subsequent chemical oxidation or reduction with $Na_2S_2O_8$ or $NaBH_4$, respectively, nor electrochemically by the application of a starting potential, thus explaining the lack of blueish coloration for any CNDs and the absence of **4** in the MS of any CNDs.

We applied the molecular insights obtained from the redox experiments with **4** to the oxidative and reductive transformations of CNDs. In water, the chemical reduction of rCNDs with $NaBH_4$ transforms the 515 nm absorption into a 560 nm shoulder (Figure 4c). The latter feature is distinctive for yCNDs. Hence, rCNDs are reductively transformed to yCNDs. Coherently, reduction of rCND under solvothermal conditions in DMF with NaOH in an autoclave for 6 h at 180 °C results in the formation of the characteristic absorptions of yCNDs (Figure 4c). The reduction is most likely caused by hydrogen formed in situ from DMF decomposition to afford formic acid, among others.[25] Formamide, which was used as a solvent for the synthesis of the CNDs, reacts with NaOH, which results in the formation of formates, and subsequently decomposes forming hydrogen (Figure S13, Supporting Information).[26] Additionally, we have conducted the synthesis of yCNDs with KOH and $Ca(OH)_2$ (see Supporting Information). The corresponding absorption spectra resemble the one of yCND. A characteristic peak at 350 nm, a shoulder at 420 nm, and a minor peak at 520 nm reinforce the previously mentioned role of the base in the solvothermal reaction (Figure S14, Supporting Information). With respect to reversibility, neither solvothermal processing of yCNDs in DMF, nor addition of chemical oxidants gives rise to the rCND absorption features. As such, recovery of the characteristic reddish coloration is ruled out (Figure S15, Supporting Information).

Finally, we characterized **4** with Raman spectroscopy and XRD and compared the results to rCND and yCND (Figure S1, Supporting Information). Interestingly, **4** itself shows very similar G- and D-bands at 1588 and 1344 cm^{-1}, respectively, with a D-to-G intensity ratio of 0.74. This suggests, that the presumed CND graphitization stems primarily from dimerization or oligomerization of **1**. The higher D-to-G intensity ratios for CNDs compared to **4** demonstrate that CNDs feature an amorphous matrix formed during the solvothermal synthesis via polycondensation reactions of citric acid, and yields an amorphous, highly branched polyester. Temperatures exceeding 120 °C have been reported to be sufficient to polymerize citric acid, which implements that it may also take place during solvothermal processing of CNDs (180 °C).[27]

Such branched polymers are known to form hydrogels that retain water. Similar phenomena were observed for rCNDs and yCNDs. None of them can be dried in vacuo, as a viscous residue is always obtained, unless purified. Centrifugation or dialysis of CNDs assisted in removing smaller sized polymers and other free molecular units to obtaining solid CND powders. Interestingly, for purified CNDs, further dialysis results in no visible light-absorbing molecules diffusing through the

dialysis bag pores of 500 Da (Figure S16, Supporting Information). In other words, the molecular building blocks must be chemically or strongly physically bound to the polymeric citric acid matrix. A likely rationale is the presence of hydroxyl and carboxyl functional groups in the citrazinic acid dimers found in rCNDs and yCNDs. The latter are the basis for condensation reactions by means of ester formation or non-covalent binding by hydrogen bonding. The different characteristics of yCND compared to rCND observed by Raman spectroscopy can be rationalized by the in situ addition of NaOH to the reaction mixture. This affects the polymerization rate of citric acid and, in turn, lowers the overall CND amorphicity. This would also explain the AFM findings, which indicate the smaller polymeric matrix of yCNDs caused by in situ NaOH addition leading to a smaller size of the nanodots.

The characteristic reflections at 23°of rCND and yCND observed during XRD analysis were also found for **4** (Figure S3, Supporting Information). All of the above suggests that the broad reflections originate from dimeric chromophores within CNDs, rather than from sp^2-hybridized domains. In addition, a sharp reflection at 27° was found for **4**, next to the reflection at 23°. This feature is, however, absent in rCND and yCNDs. It seems plausible that inclusion of the chromophores into the polymeric matrix hampers their crystallization.

2.3. Photoelectrochemical Characterization

We continued our fundamental investigations with photoelectrochemical methods to look into the electronic properties of CND-based photoelectrodes. We first established efficient photoelectrocatalytic rCND and yCND systems. For this reason, we deposited the two different CNDs onto FTO/TiO$_2$ photoelectrodes and optimized surface coverage, electrolyte composition, and applied potential. All electrode preparation and optimization steps are described in the Supporting Information. The photoelectrochemical (PEC) cell set-up includes a TiO$_2$-coated FTO-photoanode, which is sensitized with CNDs as the working electrode (WE). A Pt mesh is used as the counterelectrode (CE) and an Ag/AgCl reference electrode (RE) completes

the set-up (Figure S17, Supporting Information). The photoanode was irradiated using a Xe-lamp with a power output of 100 mW cm^{-2} coupled to a 450 nm long-pass filter to avoid TiO$_2$ photoexcitation.

An optimized stable photocurrent of 0.5 mA cm^{-2} is observed for rCNDs upon applying +0.3 V versus Ag/AgCl in an aqueous electrolyte featuring 25 vol% TEOA and 0.4 M ascorbic acid (AA) at pH 9.36. For yCND, the aqueous electrolyte consists of 15 vol% TEOA and 2.1 M AA at pH 8.74 and allows a 30% higher photocurrent of 0.7 mA cm^{-2}. The corresponding chronoamperometric transients and linear sweep voltammograms are shown in **Figure 5**a,b, respectively. Data were taken after 6 h of photoirradiation, at which time the photocurrents are maximized, as is evident from the long-term chronoamperometric measurements (Figure S18, Supporting Information). IPCE and EIS measurements were conducted in the same PEC cell with the optimized TEOA/AA electrolyte, but only with WE (FTO/TiO$_2$/CND) and CE (Pt mesh). Even though the two photoanodes possess similar patterns of light-conversion efficiency, evident by the IPCE, yCNDs are more efficient in the spectral range between 400 and 700 nm (Figure S19, Supporting Information). The same trend is evident in the EIS experiments. In the presence or absence of light, larger resistances were found for the rCND-photoelectrodes than for the yCND-photoelectrodes. Larger semicircles in the impedance spectra document this difference (Figure S20, Supporting Information). We infer that yCNDs inject electrons across the interface more efficiently than rCNDs. Such a distinction correlates well with the molecular defined oxidized/electron-deficient nature of rCNDs and reduced/electron-rich character of yCNDs.

As a complement, we performed chronoamperometric assays with rCNDs and yCNDs immobilized on FTO/NiO and FTO/TiO$_2$ photoelectrodes in a 0.5 M KH$_2$PO$_4$/K$_2$HPO$_4$ buffer without any sacrificial electron donors. The electrode preparation is described in the Supporting Information. All tests were carried out with the 3-electrode PEC cell under illumination of the WE with a 100 mW cm^{-2} Xe-lamp coupled to a 450 nm long-pass filter.

FTO/TiO$_2$/rCND data resemble what was seen for bare FTO/TiO$_2$ photoelectrodes after 25 s of photo-irradiation (**Figure 6**a).
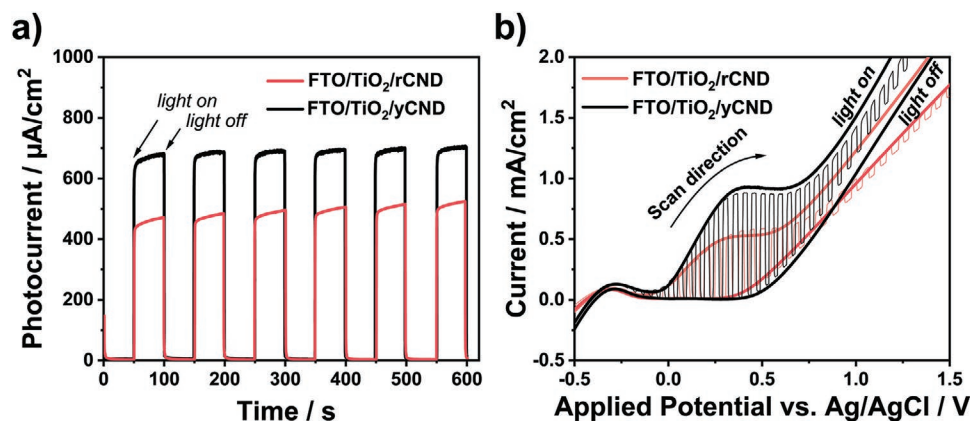

Figure 5. a) Chronoamperommetry with 50 s chopped light (100 mW cm^{-2}, 450 nm long-pass filter, U = 0.3 V vs Ag/AgCl) taken after 6 h of electrode irradiation in an optimized electrolyte composed of AA and TEOA. b) Linear sweep voltammetry (100 mW cm^{-2}, 450 nm long-pass filter, 100 mV s^{-1}) under different conditions: light on, light off, and chopped light, taken after 6 h of electrode irradiation in an optimized electrolyte composed of AA and TEOA.
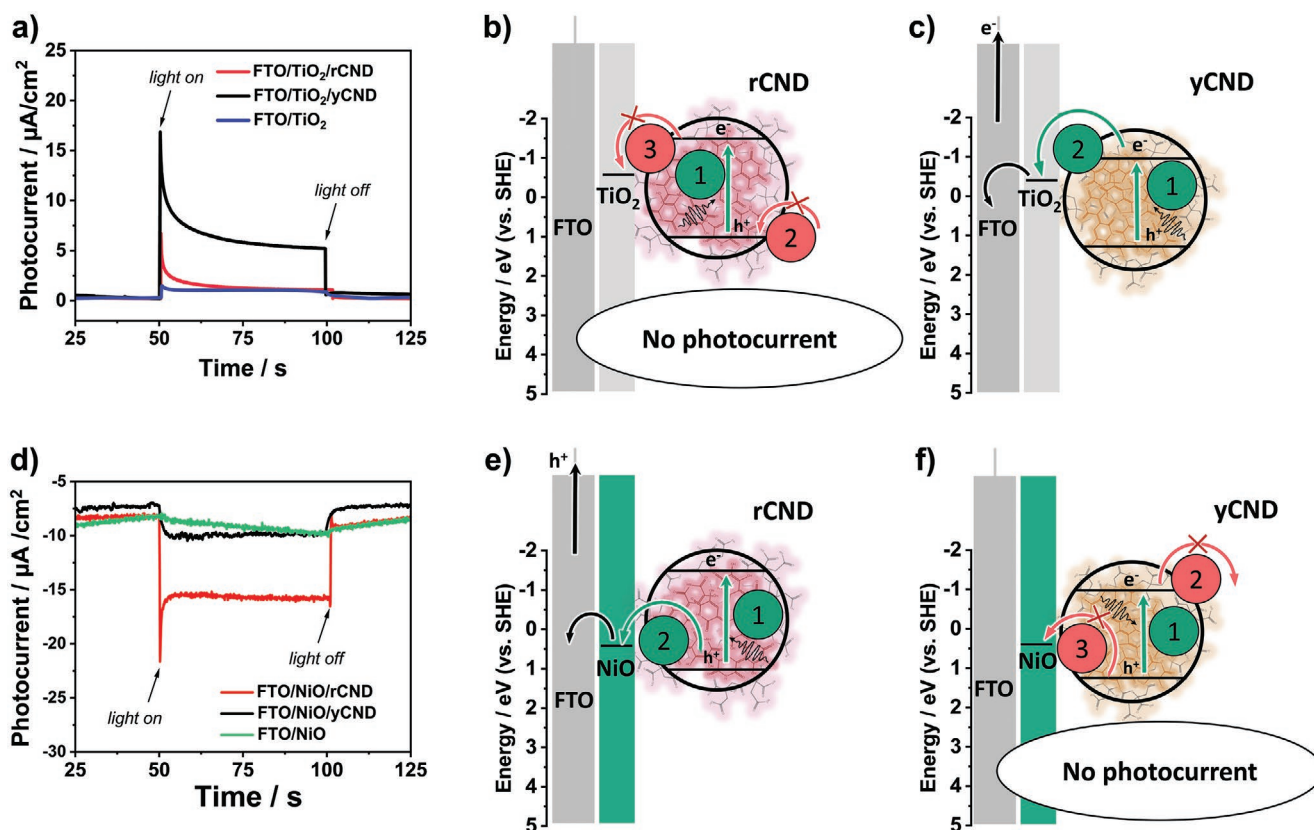
Figure 6. Chronoamperometric transients with a) TiO_2 upon application of +0.3 V versus Ag/AgCl and d) NiO upon application of −0.3 V versus Ag/AgCl. Schematic representation of photoanodic and photoelectrochemical processes in b) rCND and c) yCND on TiO_2 (top) and in e) rCND and f) yCND on NiO (bottom) with an electrolyte composed of KH_2PO_4/K_2HPO_4-buffer without any electron donor.

Thus, interfacial electron injection from rCNDs into TiO_2 is inefficient. In contrast, $FTO/TiO_2/yCND$ photoelectrodes gave rise to a remarkable 5 µA photocurrent even in the absence of any sacrificial electron donor (Figure 6a). A photocurrent flow suggests photoexcited yCNDs that inject electrons into TiO_2 without needing to be reduced first by an electron donor (Figure 6c). For rCND, on the other hand, a pre-reduction is required to trigger an interfacial electron transfer into TiO_2. Consequently, the use of an electron-donor free electrolyte fails to produce any appreciable photocurrents in the case of rCNDs (Figure 6b).

Relative to bare FTO/NiO photoelectrodes, FTO/NiO/rCNDs produce an additional photocurrent of 10 µA upon photoirradiation (Figure 6d). The ability to generate photocurrents in the absence of a sacrificial electron donor underlines the electron-poor nature of rCNDs and, hence, their ability to transfer holes to NiO upon photoexcitation (Figure 6e). In contrast, the chronoamperometric transients observed for FTO/NiO/yCNDs are barely distinguishable from those seen for bare FTO/NiO photoelectrodes (Figure 6d). This behavior is linked to the electron-rich nature of yCNDs, which prevents hole injection in NiO (Figure 6f). In conclusion, the electron-accepting ability of TiO_2 proves the electron-donating character of yCNDs, while the hole-accepting ability of NiO underlines that rCNDs are hole donors.

2.4. Time-resolved Photophysical Characterization

In the final part of our investigations, we probed visible-light driven photocurrent generation by means of transient absorption spectroscopy (TAS) and gathered mechanistic insights into the interfacial processes. CND-decorated TiO_2 slides were photoexcited at 550 nm under the conditions that were used in the PEC experiments – vide supra. TAS experiments were performed in the 3-electrode glass-PEC cell – Figure S21, Supporting Information.

TAS of rCNDs in the presence of TEOA and AA are shown in **Figure 7**a and the corresponding spectral features after selective time delays in Figure 7b. Photoexcitation of rCNDs leads to ground-state bleaching (GSB) in the region from 430 to 570 nm with a minimum at 500 nm and excited state absorption (ESA) from 570 to 750 nm with a maximum at 648 nm (Figure 7b black spectrum). Global analysis revealed that a new ESA at 550 nm evolves after 1.3 ps (Figure 7b red spectrum). The correspondingly formed second transient is long-lived and decays multiexponentially with a total ground-state recovery time of 226 µs. No further spectral changes are, however, noted throughout this slow decay (Figure S22, Supporting Information). Important is that the rise of the 550 nm ESA features similarity with the red-edge absorption feature of yCNDs (Figure 7b). In other words, rCNDs, which were per se oxidized in the solvothermal
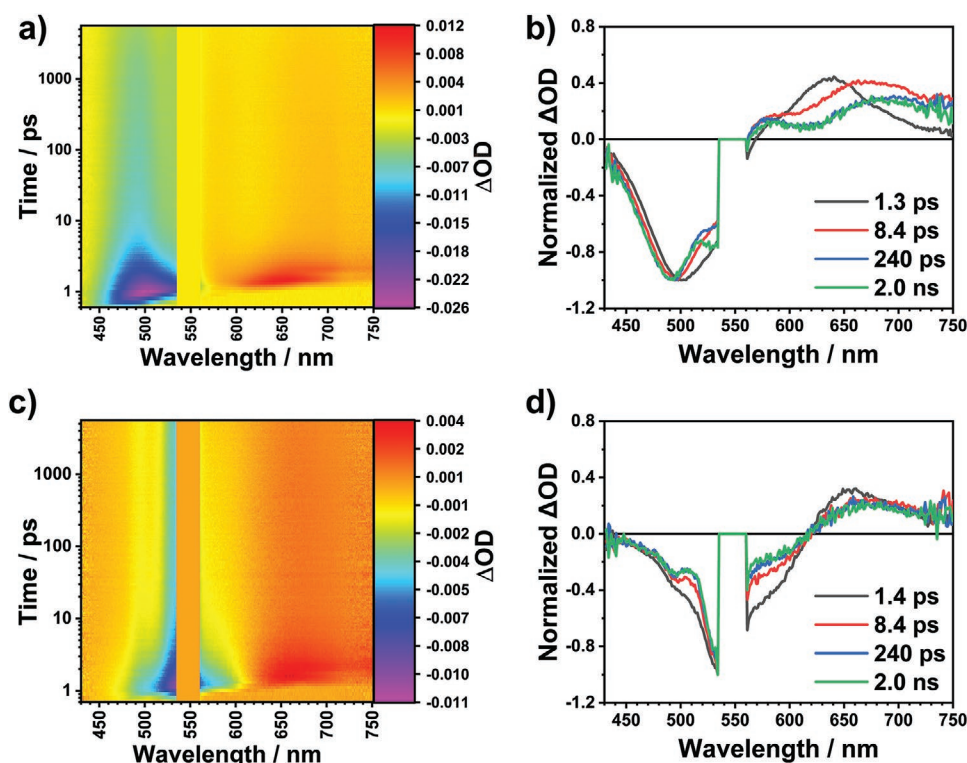
ADVANCED
SCIENCE NEWS
www.advancedsciencenews.com

NANO · MICRO
small
www.small-journal.com

Figure 7. Femtosecond transient absorption spectra after 550 nm photoexcitation of CNDs in a spectroelectrochemical set-up with an optimized electrolyte composed of AA and TEOA. a) Heat map of TAS raw data obtained in 550 nm pump-probe experiments with time delays up to 5.5 ns with rCNDs sensitized TiO$_2$ slide. b) Representative normalized spectra after various time delays, depicting the spectral changes after photoexcitation. c) Heat map of TAS raw data obtained in 550 nm pump-probe experiments with time delays up to 5.5 ns with yCNDs sensitized TiO$_2$ slide. d) Representative normalized spectra after various time delays, depicting the spectral changes after photoexcitation.

synthesis, are first reduced by either TEOA or AA after photoexcitation. Once reduced, rCNDs deactivate presumably via interfacial charge-injection into TiO$_2$. This agrees well with the observed photocurrents shown in Figure 5a. In the absence of any sacrificial electron donor, the initial rCND reduction is not seen. Instead, photoexcited rCNDs decay with an even longer ground-state recovery time of 357 µs and without the evolution of any new transients (Figures S23 and S24, Supporting Information). This explains the lack of any appreciable photocurrents for FTO/TiO$_2$/rCND when TEOA or AA are absent.

TAS experiments with yCNDs in the presence of TEOA and AA (Figure 7c) resulted in an initial GSB between 430 and 620 nm and an ESA in the region from 620 to 750 nm that maximizes at 655 nm (Figure 7d black spectrum). This initial transient gives a rise to a new ESA at 510 nm after 1.4 ps (Figure 7d red spectrum). This second transient is subject to a multi-exponential decay, by which the ground-state is repopulated. The total ground-state recovery time is 133 µs (Figure S22, Supporting Information). The 510 nm ESA features similarity with the ground-state absorption of rCNDs (Figure 1a). yCNDs, with the build-in dimers in their reduced form, are first oxidized following photoexcitation, presumably via interfacial charge-injection into TiO$_2$. These oxidized yCNDs are then reduced by means of the sacrificial electron donating TEOA and AA.

In a repeat of the TAS experiments with yCNDs, but without any sacrificial electron donors in the electrolyte solution, the

same 510 nm ESA is observed as a fingerprint of the second transient (Figures S23 and S24, Supporting Information). It takes, however, 18.8 ps rather than 1.4 ps to be formed and is of significantly lower intensity. This second transient deactivates to the ground-state multi-exponentially with a recovery time of 240 µs. By virtue of its electron-rich nature, yCNDs inject electrons into TiO$_2$ after photoexcitation as proposed in Figure 6c. Hereby, no requirement for a sacrificial electron donor is found. Ground-state deactivation is assumed to occur via interfacial charge-recombination, which is somewhat slower than the reduction by a sacrificial electron donor.

These interfacial experiments suggest that the reaction steps involved in the photocurrent generation are fundamentally different for rCND and yCND. rCNDs, which are obtained in an electron-poor form, require an initial reduction by, for example, a sacrificial electron donor before an interfacial electron injection into TiO$_2$ occurs (Figure 6b). rCNDs are intrinsic hole donors as proven in experiments with NiO (Figure 6e). yCNDs, on the other hand, are obtained in an electron-rich form and hence, inject free charge carriers in TiO$_2$ independent of the presence of sacrificial electron donors (Figure 6c). As a consequence, yCNDs are unable to produce photocurrents in combination with FTO/NiO due to their electron-rich nature and inability to donate holes at the electrode surface (Figure 6f). This implies that rCNDs are electron-poor, whereas yCND are electron-rich.
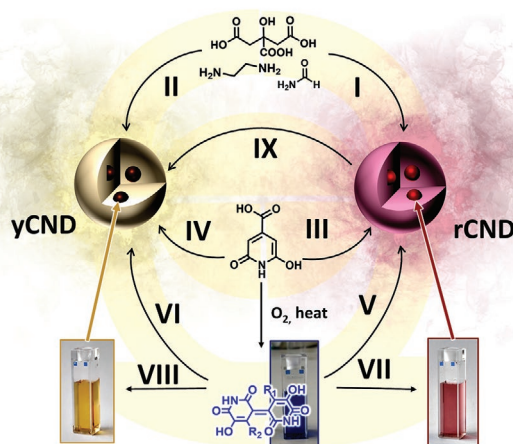
ADVANCED
SCIENCE NEWS
www.advancedsciencenews.com

NANO · MICRO
small
www.small-journal.com

Figure 8. Schematic representation of chemical and solvothermal transitions within yCNDs and rCNDs.

3. Conclusions

Visible-light absorbing CNDs were prepared by a solvothermal reaction of citric acid, ethylenediamine and formamide, affording rCNDs (**Figure 8**, reaction **I**), and by in situ addition of NaOH, affording yCNDs (Figure 8, reaction **II**). In this reaction, **1** is formed due to a ring-closing reaction between formamide and citric acid. To prove this, we treated **1** solvothermally under the synthetic conditions used to synthesize CNDs. CNDs synthesized from **1** resulted in the same spectroscopic properties as rCNDs (Figure 8, reaction **III**) and, in case of in situ addition of NaOH, as yCNDs (Figure 8, reaction **IV**).

To monitor the transition from transparent **1** to a colored chromophore, **1** was heated at 80 °C and stirred in the presence of O_2, which afforded **4**. Subsequent solvothermal treatment of **4** resulted in CNDs, whose spectroscopic properties are similar to those seen for rCNDs. Here, it is the characteristic reddish coloration that stands out (Figure 8, reaction **V**). In contrast, solvothermal processing of **4** with NaOH resulted in a yellow chromophore, which resembles yCNDs spectroscopically (Figure 8, reaction **VI**). The link between the transfer of **4** and the characteristic CND-coloration was revealed by means of (electro)chemical oxidation (Figure 8, reaction **VII**) and reduction (Figure 8, reaction **VIII**), which yielded reddish and yellowish chromophores, spectroscopically similar to rCNDs and yCNDs, respectively. Hence, NaOH added in situ mediates the reductive conditions during the solvothermal procedure. Independent confirmation came from treating rCNDs with NaOH solvothermally, which revealed the typical spectroscopic properties of yCNDs (Figure 8, reaction **IX**). These chromophores are chemically bonded to an amorphous polycitric acid matrix, building the nanosized CND-material, as evident from AFM and post-synthetic dialysis test.

Additional tests with TiO_2 and NiO in the absence and presence of electron donors corroborated that rCNDs and yCNDs are electron-poor and electron-rich, respectively. The electron donating nature of yCNDs, for example, increases the photocurrent performance relative to $FTO/TiO_2/rCNDs$

photoelectrodes by 30%. On the other hand, rCNDs require pre-reduction after photoexcitation to generate any sizeable photocurrents.

Supporting Information

Supporting Information is available from the Wiley Online Library or from the author.

Acknowledgements

Conflict of Interest

The authors declare no conflict of interest.

Author Contributions

Y.R., B.J., D.L., A.C., and D.G. conceived the project. Y.R., B.J., and X.Z. performed synthesis and steady-state spectroscopy experiments. Y.R. and P.S. conducted electrochemical and photoelectrochemical characterization. D.L. conducted transient-absorption spectroscopy. M.K. and T.D. characterized the CNDs by means of mass spectrometry, R.C. by means of XRD experiments, T.S. by means of AFM. T.C and Y.B conducted the theoretical calculations. Y.R., B.J., and D.L. main-authored the manuscript, A.C. and D.G. co-contributed to the manuscript. All authors contributed to fruitful discussions of the results and revisions of the manuscript.

Data Availability Statement

Research data are not shared.

Keywords

[1] a) W.-H. Chen, J. E. Lee, S.-H. Jang, S.-S. Lam, G. H. Rhee, K.-J. Jeon, M. Hussain, Y.-K. Park, *Int. J. Energy Res.* **2022**, *46*, 5467; b) S.-C. Yiu, P.-Y. Ho, Y.-Y. Kwok, X. He, Y. Wang, W.-H. Yu, C.-L. Ho, S. Huang, *Chem. -Eur. J.* **2022**, *28*, e202104575; c) R. Gao, L. Xiong, X. Li, W. Chen, L. Mao, *Int. J. Hydrogen Energy* **2022**, *47*, 20825.

[2] a) B. C. M. Martindale, G. A. M. Hutton, C. A. Caputo, E. Reisner, *J. Am. Chem. Soc.* **2015**, *137*, 6018; b) J. B. Essner, G. A. Baker, *Environ. Sci.: Nano* **2017**, *4*, 1216.

[3] S. Liao, X. Zhao, F. Zhu, M. Chen, Z. Wu, X. song, H. Yang, X. Chen, *Talanta* **2018**, *180*, 300.

[4] H. Wang, F. Lu, C. Ma, Y. Ma, M. Zhang, B. Wang, Y. Zhang, Y. Liu, H. Huang, Z. Kang, *J. Mater. Chem. B* **2021**, *9*, 125.

[5] a) H. Shibata, M. Abe, K. Sato, K. Uwai, K. Tokuraku, T. Iimori, *Carbohydr. Polym. Technol. Appl.* **2022**, *3*, 100218; b) V. Strauss, J. T. Margraf, T. Clark, D. M. Guldi, *Chem. Sci.* **2015**, *6*, 6878; c) V. Strauss, J. T. Margraf, C. Dolle, B. Butz, T. J. Nacken, J. Walter, W. Bauer, W. Peukert, E. Spiecker, T. Clark, D. M. Guldi, *J. Am. Chem. Soc.* **2014**, *136*, 17308.

[6] D. Zhou, P. Jing, Y. Wang, Y. Zhai, D. Li, Y. Xiong, A. V. Baranov, S. Qu, A. L. Rogach, *Nanoscale Horiz.* **2019**, *4*, 388.

[7] V. Hinterberger, C. Damm, P. Haines, D. M. Guldi, W. Peukert, *Nanoscale* **2019**, *11*, 8464.

[8] a) W. Wang, B. Wang, H. Embrechts, C. Damm, A. Cadranel, V. Strauss, M. Distaso, V. Hinterberger, D. M. Guldi, W. Peukert, *RSC Adv.* **2017**, *7*, 24771; b) S. Xie, X. Li, L. Wang, F. Zhu, X. Zhao, T. Yuan, Q. Liu, X. Chen, *Microchem. J.* **2021**, *160*, 105718; c) X. Zhao, L. Wang, Q. Liu, M. Chen, X. Chen, *Microchem. J.* **2021**, *163*, 105888.

[9] H. Ding, J.-S. Wei, N. Zhong, Q.-Y. Gao, H.-M. Xiong, *Langmuir* **2017**, *33*, 12635.

[10] J. T. Margraf, F. Lodermeyer, V. Strauss, P. Haines, J. Walter, W. Peukert, R. D. Costa, T. Clark, D. M. Guldi, *Nanoscale Horiz.* **2016**, *1*, 220.

[11] a) G. Gyulai, F. Ouanzi, I. Bertóti, M. Mohai, T. Kolonits, K. Horváti, S. Bősze, *J. Colloid Interface Sci.* **2019**, *549*, 150; b) Z. Tian, X. Zhang, D. Li, D. Zhou, P. Jing, D. Shen, S. Qu, R. Zboril, A. L. Rogach, *Adv. Opt. Mater.* **2017**, *5*, 1700416.

[12] a) Y. Yan, L. Xia, L. Ma, *RSC Adv.* **2019**, *9*, 24057;. b) K. Holá, M. Sudolská, S. Kalytchuk, D. Nachtigallová, A. L. Rogach, M. Otyepka, R. Zbořil, *ACS Nano* **2017**, *11*, 12402.

[13] W. Liang, P. Wang, M. J. Meziani, L. Ge, L. Yang, A. K. Patel, S. O. Morgan, Y.-P. Sun, *Nanoscale Adv.* **2021**, *3*, 4186.

[14] Y. Zhang, Y. Cui, P. Chen, S. Liu, N. Zhou, K. Ding, L. Fan, P. Peng, M. Min, Y. Cheng, Y. Wang, Y. Wan, Y. Liu, B. Li, R. Ruan, in *Sustainable Resource Recovery and Zero Waste Approaches*, Vol. *1*,

(Eds: M. J. Taherzadeh, K. Bolton, J. Wong, A. Pandey), Elsevier, St. Louis, MO **2019**.

[15] C. Li, Y. Wang, X. Zhang, X. Guo, X. Kang, L. Du, Y. Liu, *J. Colloid Interface Sci.* **2018**, *526*, 487.

[16] a) Y. Hu, J. Yang, J. Tian, J.-S. Yu, *J. Mater. Chem. B* **2015**, *3*, 5608; b) D. S. Franklin, S. Guhanathan, *Polym. Bull.* **2014**, *71*, 93.

[17] A. Soewono, S. Rogak, *Aerosol Sci. Technol.* **2011**, *45*, 1206.

[18] A. Sadezky, H. Muckenhuber, H. Grothe, R. Niessner, U. Pöschl, *Carbon* **2005**, *43*, 1731.

[19] K. J. Mintz, M. Bartoli, M. Rovere, Y. Zhou, S. D. Hettiarachchi, S. Paudyal, J. Chen, J. B. Domena, P. Y. Liyanage, R. Sampson, D. Khadka, R. R. Pandey, S. Huang, C. C. Chusuei, A. Tagliaferro, R. M. Leblanc, *Carbon* **2021**, *173*, 433.

[20] P. Duan, B. Zhi, L. Coburn, C. L. Haynes, K. Schmidt-Rohr, *Magn. Reson. Chem.* **2020**, *58*, 1130.

[21] Y. Song, S. Zhu, S. Zhang, Y. Fu, L. Wang, X. Zhao, B. Yang, *J. Mater. Chem. C* **2015**, *3*, 5976.

[22] a) B. Jana, Y. Reva, T. Scharl, V. Strauss, A. Cadranel, D. M. Guldi, *J. Am. Chem. Soc.* **2021**, *143*, 20122; b) W. Kasprzyk, T. Świergosz, S. Bednarz, K. Walas, N. V. Bashmakova, D. Bogdał, *Nanoscale* **2018**, *10*, 13889; c) A. Sharma, T. Gadly, S. Neogy, S. K. Ghosh, M. Kumbhakar, *J. Phys. Chem. Lett.* **2017**, *8*, 1044.

[23] V. Strauss, H. Wang, S. Delacroix, M. Ledendecker, P. Wessig, *Chem. Sci.* **2020**, *11*, 8256.

[24] a) J. C. Ensign, S. C. Rittenberg, *Arch. Microbiol.* **1965**, *51*, 384; b) J. Lee, U. von Gunten, J.-H. Kim, *Environ. Sci. Technol.* **2020**, *54*, 3064.

[25] a) J. K. Magtaan, M. Devocelle, F. Kelleher, *J. Pept. Sci.* **2019**, *25*, e3139; b) J. Yu, P. E. Savage, *Ind. Eng. Chem. Res.* **1998**, *37*, 2.

[26] a) T. Meisel, Z. Halmos, K. Seybold, E. Pungor, *J. Therm. Anal.* **1975**, *7*, 73; b) W. Balcerowiak, *Thermochim. Acta* **1985**, *92*, 661.

[27] M. Wrzecionek, G. Matyszczak, A. Bandzerewicz, P. Ruśkowski, A. Gadomska-Gajadhur, *Org. Process Res. Dev.* **2021**, *25*, 271.